PUBLICATION VI

Parametric dependences of momentum pinch and Prandtl number in JET

In: Nuclear Fusion 51, 123002 (11 pp), 2011.

http://iopscience.iop.org/0029-5515/51/12/123002/pdf/0029-5515_51_12_123002.pdf

IOP Publishing and International Atomic Energy Agency Nuclear Fusion

Nucl. Fusion **51** (2011) 123002 (11pp) doi:10.1088/0029-5515/51/12/123002

Parametric dependences of momentum pinch and Prandtl number in JET

T. Tala[1], A. Salmi[2], C. Angioni[3], F.J. Casson[3], G. Corrigan[4], J. Ferreira[5], C. Giroud[4], P. Mantica[6], V. Naulin[7], A.G. Peeters[8], W.M. Solomon[9], D. Strintzi[8], M. Tsalas[10], T.W. Versloot[10], P.C. de Vries[10], K.-D. Zastrow[4] and JET-EFDA contributors[a]

JET-EFDA, Culham Science Centre, OX14 3DB, Abingdon, UK
[1] Association EURATOM-Tekes, VTT, PO Box 1000, FIN-02044 VTT, Finland
[2] Association EURATOM-Tekes, Aalto University, Department of Applied Physics, Finland
[3] Max-Planck-Iinstitut für Plasmaphysik, EURATOM-Assoziation, Garching, Germany
[4] EURATOM/CCFE Fusion Association, Culham Science Centre, Oxon. OX14 3DB, UK
[5] Associação EURATOM/IST, Instituto de Plasmas e Fusao Nuclear, 1049-001 Lisbon, Portugal
[6] Istituto di Fisica del Plasma CNR-EURATOM, via Cozzi 53, 20125 Milano, Italy
[7] Association Euratom-Risø-DTU, Denmark
[8] Physics Department, University of Bayreuth, 95440 Bayreuth, Germany
[9] Princeton Plasma Physics Laboratory, Princeton University, Princeton, NJ 08543, USA
[10] FOM Institute Rijnhuizen, Association EURATOM-FOM, Nieuwegein, The Netherlands

E-mail: tuomas.tala@vtt.fi

Received 21 June 2011, accepted for publication 7 October 2011
Published 7 November 2011
Online at stacks.iop.org/NF/51/123002

Abstract
Several parametric scans have been performed to study momentum transport on JET. A neutral beam injection modulation technique has been applied to separate the diffusive and convective momentum transport terms. The magnitude of the inward momentum pinch depends strongly on the inverse density gradient length, with an experimental scaling for the pinch number being $-Rv_{\mathrm{pinch}}/\chi_\phi = 1.2R/L_{\mathrm{n}} + 1.4$. There is no dependence of the pinch number on collisionality, whereas the pinch seems to depend weakly on q-profile, the pinch number decreasing with increasing q. The Prandtl number was not found to depend either on R/L_{n}, collisionality or on q. The gyro-kinetic simulations show qualitatively similar dependence of the pinch number on R/L_{n}, but the dependence is weaker in the simulations. Gyro-kinetic simulations do not find any clear parametric dependence in the Prandtl number, in agreement with experiments, but the experimental values are larger than the simulated ones, in particular in L-mode plasmas. The extrapolation of these results to ITER illustrates that at large enough $R/L_{\mathrm{n}} > 2$ the pinch number becomes large enough (>3–4) to make the rotation profile peaked, provided that the edge rotation is non-zero. And this rotation peaking can be achieved with small or even with no core torque source. The absolute value of the core rotation is still very challenging to predict partly due to the lack of the present knowledge of the rotation at the plasma edge, partly due to insufficient understanding of 3D effects like braking and partly due to the uncertainties in the extrapolation of the present momentum transport results to a larger device.

(Some figures may appear in colour only in the online journal)

1. Introduction

Plasma rotation and momentum transport are currently very active areas of research, both experimentally and theoretically. It is well known that sheared plasma rotation can stabilize turbulence [1–4] while the rotation itself has beneficial effects on MHD modes, such as resistive wall modes or neoclassical tearing modes (NTMs) [5, 6]. Although the importance of rotation has been recently recognized, predicting or extrapolating the toroidal rotation profile has turned out to be extremely challenging and several key issues remain. The uncertainties in the predictions can be classified into the following three main categories: core torque sources and sinks, edge rotation and sources/sinks and momentum transport.

The neutral beam injection (NBI) torque source is relatively well established, and a lot of work has been

[a] See the appendix of Romanelli F. *et al* 2011 *Nucl. Fusion* **51** 094008.

performed recently to compare and benchmark different codes [7, 8]. These benchmark activities have been performed to be sure that the torque calculation between different codes agrees well so that no significant error is propagated into the momentum transport analysis when analysing NBI modulation experiments. The NBI torque calculation is believed to be understood even with a large toroidal magnetic field ripple amplitude. The NBI torque calculation in plasmas with large ripple has been recently benchmarked against JET experiments and good agreement has been found [8]. The most important effect of the NBI on rotation in plasmas with a ripple on JET was found to be due to non-ambipolar fast ion losses, causing a counter current torque on the plasma [9].

In addition to NBI, other core torque sources and sinks are less understood. Intrinsic rotation in ICRH, ECRH and ohmic plasmas still requires clarification [10–12]. In JET, in plasmas with the usual ripple of $\delta = 0.08\%$, the angular frequency of the intrinsic rotation is less than $\omega_\phi < \pm 10\,\mathrm{krad\,s^{-1}}$ [13]. The ripple also affects the angular rotation frequency under the conditions of no external momentum input. The ripple amplitude was varied from $\delta = 0.08\%$ to $\delta = 1.5\%$ in ohmic and ICRH heated plasmas. Ripple affects both the edge rotation by lowering it typically close to zero or to small counter-rotation values and also the core rotation where it becomes counter-rotating [14]. In addition to the effect of ripple on fast ions, as rotation in ohmic plasmas was also affected by the magnitude of the ripple, there is evidence that thermal ions are influenced by the ripple, being an indication of an neoclassical toroidal viscosity (NTV) type of process in place with a large enough ripple. This NTV is also present in NBI and ICRH heated plasmas with ripple, but its influence on rotation is masked to a large extent by the effect of fast ions on rotation. Recently, an experiment to study mode conversion flow drive (MCFD) was also performed in L-mode plasmas using a He^3 ICRH scheme [15]. MCFD was found to be sensitive to the He^3 concentration level. Large central counter-rotation up to $\omega_\phi = -10\,\mathrm{krad\,s^{-1}}$ ($v_\phi = -30\,\mathrm{km\,s^{-1}}$) was observed at He^3 concentration levels of 10–17%. The physical mechanism of MCFD is not yet completely understood, but clearly some core torque source exists, as also found in MCFD experiment on C-Mod [16].

Another unknown torque source in the core plasma, probably also being very important in ITER rotation predictions, is seen as a strong toroidal rotation braking in plasmas with application of an $n = 1$ magnetic perturbation field on JET [17]. The maximum value (typically about half of the NBI torque) of the torque is at the plasma central region ($\rho < 0.4$). Moreover, it is not localized at certain magnetic surfaces, indicating that the non-resonant component dominates over the resonant magnetic braking. The NTV calculation shows that in these JET plasmas the calculated NTV torque profile is an order of magnitude smaller than the experimentally observed torque profile T_{EFCC}, indicative of a core torque source that is far from fully understood. NTV type of torque has been observed earlier also for example on DIII-D [18]. In addition to the magnetic perturbation coils, there is evidence from DIII-D that the test blanket modules (TBMs) may have a very large effect on plasma rotation in the plasma core [19].

The second major issue in giving large uncertainties in ITER rotation predictions is the lack of the knowledge of the edge rotation as well as edge torque sources. In principle, there is a similar problem in predicting the rotation profile as predicting the temperature profile—the boundary/pedestal value must be known accurately in order to predict the toroidal rotation profile in the core plasma. Recently, the loss of plasma toroidal angular momentum and thermal energy due to edge localized modes (ELMs) has been studied in JET. The analysis shows a consistently larger drop in momentum in comparison with the energy loss associated with the ELMs under a wide variety of plasma conditions [20]. Another edge uncertainty is the charge-exchange interaction between the plasma ions and the neutral particle background creating a continuous sink of momentum and energy. The magnitude of CX losses increases to approximately 10% of the total input torque with the power losses being smaller with an increasing amount of neutrals [21]. Additional known uncertainties in the edge rotation and torque sources are, for example, due to toroidal magnetic field ripple [9], TBMs [19] and interaction with SOL flows, seen for example between the upper and lower null configurations on C-Mod [22, 23] and a term in the momentum flux called residual stress [24].

While the core and edge torque sources and the edge rotation question are crucial in order to be able to predict the rotation profile in future tokamaks, in this paper we concentrate on core momentum transport studies. The momentum diffusivity χ_ϕ and pinch velocity v_{pinch} (negative sign denotes inwards) are related to the toroidal velocity v_ϕ, its gradient ∇v_ϕ and the momentum flux Γ_ϕ, assuming the absence of a significant particle flux, as follows:

$$\Gamma_\phi \sim -n\chi_\phi \nabla v_\phi + n v_{\mathrm{pinch}} v_\phi = -n\chi_\phi^{\mathrm{eff}} \nabla v_\phi \qquad (1)$$

where n is the ion density. The diffusive and convective part of the momentum flux can be combined into an effective momentum diffusivity χ_ϕ^{eff}, which can be calculated from steady-state rotation profiles once momentum sources are known. This equation is a simplification of the actual momentum flux as it includes only terms proportional to the gradient of the rotation or the rotation itself. There is a term missing in equation (1) called a residual stress [24] that refers to the part of the momentum flux which is not diffusive or pinch. Studies of the residual stress term is beyond the scope of this work, with the exception of a comment on the possible role of a residual stress in this analysis and a term proportional to the $E \times B$ shear [25] based on gyro-kinetic simulations. There is a comprehensive recent overview of toroidal momentum transport with all flux terms described in detail in [26]. The best and most clean way of identifying separately diffusive and convective transport components is by means of perturbative experiments, i.e. exploiting the additional information contained in the dynamic response of the plasma rotation to a time variation of the torque source. Perturbating the rotation has been successfully applied to momentum transport studies using NBI modulation or magnetic perturbations on several tokamaks. In particular, it has been possible to demonstrate the existence of the momentum pinch on JT-60U [27], JET [7, 28–30], DIII-D [31] and NSTX [32, 33]. In all of these studies although the pinch and diffusive components were separated, no systematic studies have been experimentally carried out to study the parametric dependences of the momentum pinch and diffusive

terms. In order to understand how the pinch and diffusive terms extrapolate for example to ITER from the present tokamaks, parametric dependences of those parameters must be known, and this is the main scope of this paper.

From the theoretical point of view, the existence of the momentum pinch is also evident [34, 35]. According to theory, momentum pinch is expected to depend strongly on the inverse density gradient length R/L_n and weakly on q [26, 34]. The dependence of the momentum pinch on collisionality is found to be almost negligible [36]. The dependence of the Prandtl number on any of the parameters is expected to be small, certainly smaller than that of the momentum pinch [26]. As a consequence, the main parametric dependences studied in this work are R/L_n, collisionality ν^* and q-profile. In addition, a comparison between the H-mode and L-mode plasmas is performed.

The content of the paper is organized as follows. The experimental details, such as the NBI modulation technique, the momentum transport analysis and the NBI torque calculation are described in section 2. The results from the experimental scan to study momentum transport are described in detail in section 3. The experiment to study the collisionality dependence is presented in section 3.1. In section 3.2, the results on the R/L_n scan is summarized. Section 3.3 is devoted to the q-profile scan. The difference in momentum transport between L-mode and H-mode plasmas is shown in section 4. The role of the inward momentum pinch and the rotation boundary conditions in ITER extrapolation of the toroidal rotation is illustrated in section 5. Section 6 summarizes the main results of this paper.

2. Experimental set-up to exploit NBI modulation technique for momentum transport studies

The NBI modulation experiments have been carried out in different types of JET plasmas to study the parametric dependences of momentum pinch and Prandtl numbers. Most of the plasmas in these scans are in the following parameter regime: low collisionality JET H-mode plasmas at $B_T = 3$ T, $I_p = 1.5$ MA and $n_{e0} \sim 4 \times 10^{19}$ m^{-3}. This is combined with a minimum level of MHD activity to prevent interference with the perturbation analysis, i.e. at high $q_{95} \sim 7$ to avoid large sawteeth in the centre and with type III ELMs to avoid large periodic edge crashes. Total power levels were up to 15 MW for NBI, including the modulation, and 0–4 MW for ICRH in H minority scheme. Some of the pulses were performed with much less power (∼4–5 MW) so that they stayed in L-mode. Both in L-mode and H-mode plasmas with NBI modulation, ion temperature gradients (ITGs) are the dominant instability on JET. As the Prandtl number is defined as $P_r = \chi_\phi/\chi_i$, i.e. inversely proportional to the ion heat diffusivity, a comparison of the Prandtl number between different plasmas is more unambiguous in ITG dominated plasmas where momentum and ion heat transport are tightly coupled. In TEM dominated plasmas or in plasmas where collisional heat transfer between ions and electrons is significant, momentum and ion heat transport are less coupled, thus making $P_r = \chi_\phi/\chi_i$ a less relevant parameter to characterize momentum transport and compare different discharges and parametric dependences.

The NBI torque source is the only available tool for inducing a significant rotation modulation in JET, although it is not ideal because its deposition profile is very broad, which is a complicating factor in the analysis, unlike in the case of localized RF heat sources. On the other hand, the torque sources from NBI can be calculated more precisely than the radio-frequency power sources. A detailed description of the use of the NBI modulation technique and momentum transfer from the fast NBI ions to the bulk is presented in [7, 29].

In these JET experiments, the NBI power and torque were square wave modulated with a duty cycle of either 50% or 33% at a frequency $f_{mod} = 6.25$ Hz or $f_{mod} = 8.33$ Hz, which is the highest technically possible. This frequency is high enough to make the $\boldsymbol{J} \times \boldsymbol{B}$ torque the dominant source of torque perturbation everywhere outside $r/a > 0.3$. The modulation cycle is, on the other hand, much longer than the 10 ms time resolution of the charge exchange recombination spectroscopy (CXRS) diagnostic used to measuring the toroidal rotation profile ω_ϕ and ion temperature T_i at 12 radial points [37]. The modulated power varies from 2 to 5 MW, the power tuned to create an appropriate size of the rotation modulation amplitude of around 5%. Consequently, it is possible to observe changes in toroidal rotation in the beam on and beam off periods and perform the Fourier analysis of the modulated rotation. The modulation takes place in a stationary phase for 5–6 s. One can therefore choose the most stationary phase of the shot, with respect to density or temperature variation, to carry out the momentum transport analysis because typically some 10–20 modulation cycles (1–2 s) give enough statistics for the standard fast Fourier transformation (FFT) analysis. FFT has been applied to experimental time traces at various radial positions of ω_ϕ, T_i and T_e, to derive spatial profiles of amplitude (A) and phase (φ) of the perturbation.

Due to the absence of a torque source free region where the transport analysis could be performed independent of the details of the source, the calculation of the time-dependent torque profile is an essential step for the derivation of the momentum transport coefficients from the data. The transport analysis will in fact rely on full momentum transport simulations in which the torque source is assumed to be known precisely enough, with the obvious consequence that any error in the source will cause an error on the derived transport coefficients. It is to be noted here that the NBI torque is the only torque source taken into account in this analysis. Thus the following terms are ignored that could affect the results presented in this paper: residual stress, direct ICRH driven torque (only two of the analysed shots have ICRH, with zero phasing it ought to be small) and possible torque sources/sinks due to MHD such as ELMs or NTMs. The analysed plasmas were with type III ELMs and the NTM activity varied from zero to very mild, thus the torque originating from these is negligible as compared with the large NBI torque. The possible role of the residual stress term is discussed later in the paper.

For the calculation of NBI torque, great care has then been dedicated to such calculations and associated uncertainties. Either the TRANSP code [38] or the ASCOT code [39] has been used to calculate NBI power and torque profiles as a function of time, given the time-dependent experimental profiles of all plasma parameters (T_i from CXRS, T_e from the electron cyclotron emission (ECE) radiometer and LIDAR

or high resolution Thomson scattering (HRTS), n_e from interferometer and LIDAR or HRTS, Z_{eff} from CXRS and spectroscopic measurements and q from EFIT constrained with MSE). In order to confirm the consistency of the torque calculations, the time-dependent torque profile calculation between TRANSP and ASCOT has been benchmarked against each other in JET plasmas with NBI modulation both in [7, 8]. The agreement between the two different codes is very good and constitutes a powerful confirmation that we can rely on the torque calculations for our transport analysis.

The modulated NBI torque source is broad. Therefore, a simple determination of the momentum diffusivity and pinch directly from the spatial derivatives of the amplitude and phase of the modulated ω_ϕ is not viable. As a consequence, time-dependent transport modelling of ω_ϕ is required to extract the transport properties from the plasma dynamic response, assuming that torque sources are known with reasonable accuracy from numerical calculations. The transport analysis methodology is in this study to determine the momentum diffusivity and pinch is the same as that described in more detail in [7, 29]. It is based on predictive transport simulations of toroidal rotation using the 1.5D code JETTO [40] and the power and torque sources calculated by TRANSP or ASCOT. The transport equation for ω_ϕ is solved while q-profile, T_i, T_e and n_e are frozen to their experimental values. The boundary conditions for steady-state ω_ϕ, amplitudes $A(\omega_\phi)$ and phases $\varphi(\omega_\phi)$ of the modulated ω_ϕ are chosen to fit the experimental data at $\rho = 0.8$ as the edge momentum plasma transport is beyond the scope of interest in this study. The analysis technique is based on minimizing the error between the experimental and simulated amplitude, phase and steady-state profiles of the rotation where the transport model for the rotation includes a Prandtl number and a pinch term chosen in a way to best reproduce the experimental amplitude, phase and steady-state profiles. As a result, a Prandtl and a pinch profile covering radially the whole region from the centre up to $\rho = 0.8$ is obtained.

3. Experimental scans to study the parametric dependences of momentum transport

3.1. Collisionality scan of the momentum pinch and Prandtl numbers on JET

A 3-point collisionality scan to study momentum transport coefficients has been performed on JET. The standard method to carry out the dimensionless similarity experiment to scan the collisionality, presented in [41], has been exploited in this experiment. The main idea is to vary collisionality while keeping the other dimensionless quantities, such as ρ^*, β_N, q and T_i/T_e, as constant as possible. The collisionality is varied by changing the electron temperature using the NBI power at constant density; ρ^* and β_N are kept constant by changing the magnetic field B_t and finally q kept constant by a relevant correction in the plasma current I_p. The time traces of the most relevant quantities are shown in figure 1. Within the 3-point scan, collisionality changes over almost a factor of 4. The volume-averaged ρ^* and β_N are changing within the scan by about 10% and 20%, respectively. The NBI power modulation and the different power levels between the pulses, required

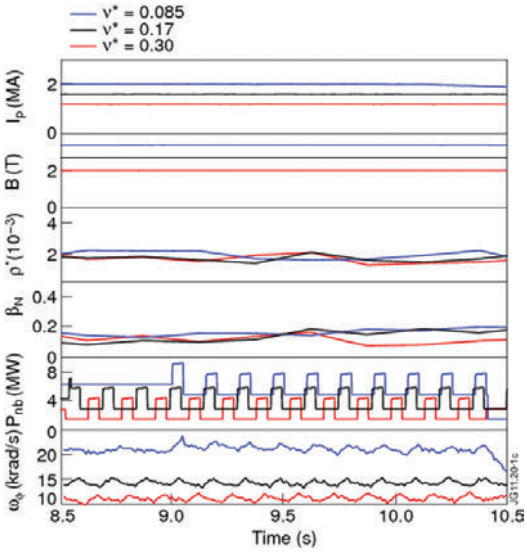

Figure 1. Time traces of plasma current I_p, magnetic field B at magnetic axis, ρ^*, β_N, NBI power P_{nb} and toroidal angular frequency ω_ϕ at $r/a = 0.5$ for 3 JET pulses no 79811 (blue), 79815 (black) and 79814 (red). The volume-averaged collisionality is also shown for each discharge.

to obtain the collisionality variation, are also shown. A clear modulated toroidal rotation ω_ϕ signal is also visible in figure 1.

The two key profiles to be kept constant within the scan in view of momentum transport studies are the density profile and the q-profile. These are both believed to play a major role in determining the magnitude of the momentum pinch in theory [34] and therefore, in order to obtain as clean as possible collisionality scan, any variations in these profiles are to be minimized. The density from the HRTS diagnostics and q-profiles from EFIT+MSE for these three shots are illustrated in figure 2, demonstrating nicely indeed that the scan succeeded well in keeping these profiles nearly identical. Both of the electron temperature profiles from ECE and the ion temperature profiles from CXRS are shown, indicating from where the difference in the collisionality between the shots originates. Also, the temperature ratio T_i/T_e is very well kept nearly constant and close to one.

The resulting Prandtl number and momentum pinch number profiles from the detailed transport analysis are shown in figure 3. It can be easily seen within the error bars from figure 3 that neither the Prandtl nor the momentum pinch number depends on collisionality. This scan was carried out in L-mode in plasmas because the collisionality scan, while simultaneously keeping R/L_n constant, is not viable to carry out in H-mode plasmas due to the density peaking dependence on collisionality [42, 43]. However, according to GS2 [44] linear gyro-kinetic simulations, these NBI heated L-mode plasmas are dominated by the ITG mode in a very similar way as those NBI heated JET plasmas in H-mode.

The magnitude of the momentum pinch numbers, ranging between 3 and 5 in the core region ($0.3 < \rho < 0.8$), in these L-mode plasmas is of the same order as found earlier

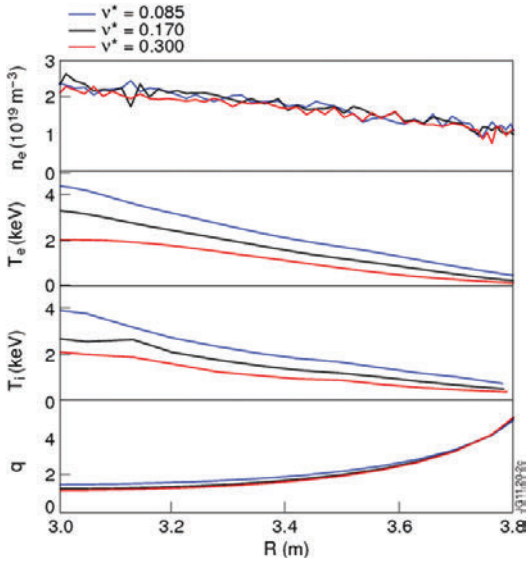

Figure 2. The radial profiles of density n_e, electron temperature T_e, ion temperature T_i and q-profile for the same shots as in figure 1 using the same colour code.

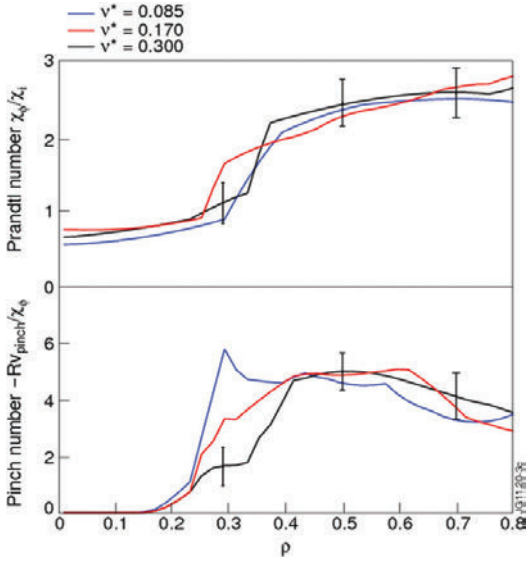

Figure 3. Prandtl number (upper frame) and pinch number (lower frame) profiles for the discharges forming the 3-point collisionality scan as a function of normalized toroidal flux co-ordinate ρ.

for most JET H-mode plasmas [7, 28, 29]. On the other hand, the Prandtl numbers tend to be some 20–40% higher in these L-mode plasmas than those of H-mode plasmas. This is discussed in more detail in section 4. There is a strong radial dependence for the Prandtl numbers, typically an increase of about a factor of 2 occurring when going from $r/a = 0.3$ to $r/a = 0.8$. It is to be noted that in the central region ($\rho < 0.2$),

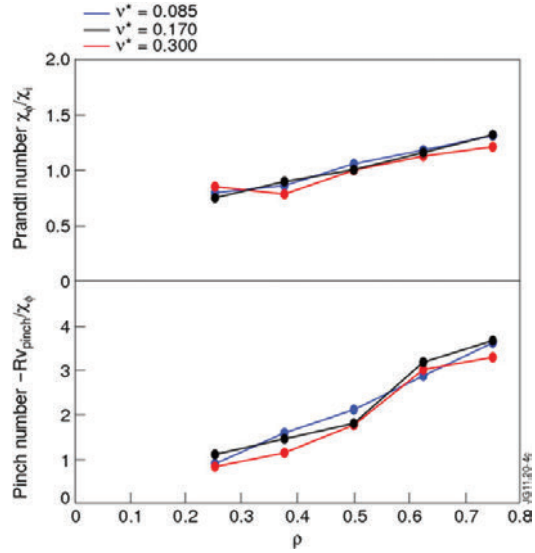

Figure 4. As in figure 3, but the data are from linear GS2 simulations using the actual input data from each shot. The GS2 runs have been performed at five radial locations for each shot.

the ITG turbulence is stable and thus, the pinch vanishes and the Prandtl number becomes close to unity for all JET shots, more or less independent of plasma parameters.

Calculation of the error bars for the Prandtl and pinch numbers using the analysis method described in detail in the references is not straightforward. In this paper, they have been estimated in such a way that first, a total error, resulting from the difference between the experimental amplitude, phase and steady-state and the simulated ones, using the choice of Prandtl and pinch number profiles that minimizes the error, has been calculated. The total error consists of the least square sum between the experimental and simulated amplitude, phase and steady-state profiles. Then, the actual error bars for P_r and $-Rv_{\mathrm{pinch}}/\chi_\phi$ have been estimated by allowing the Prandtl and pinch number profiles vary as far as the total summed error is still within 10% from the minimum total error (coming from the best choice of Prandtl and pinch numbers). The error bars shown in figure 3 and in the rest of the paper are based on this calculation method. By varying the Prandtl and pinch number profiles within the error bar range, typically the amplitude and steady-state vary by about 10–15% and the phase by about 15°, i.e. 5–10 ms. These numbers reflect well the error bars originating from the CXRS diagnostics itself (typically of the order of 5%) [45]. In addition, the experimental error in the amplitude of the modulated rotation is typically about 10%, calculated from the Fourier spectrum by taking any non-harmonic NBI modulation frequency. More details on the error bars and their calculation for the NBI modulation technique can be found in [7, 8].

The dependence of the momentum pinch and Prandtl number on collisionality was also studied in linear gyro-kinetic simulations using the GS2 code [44, 46, 47]. The GS2 runs have been performed using the actual data from each shot. The GS2 calculations were performed on a spectrum 6 modes

ranging from 0.15 to 0.8, with log spacing, and a spectral shape along [48] was used. This choice gives the usual peaking around $k_y\rho_i = 0.25$. The most important conclusion is that neither momentum pinch nor the Prandtl number depends on collisionality as illustrated clearly in figure 4. This result that the pinch and Prandtl numbers do not depend on collisionality is recently found to be valid more generally in momentum transport theory [36]. These simulation results are also fully consistent with the experimental results. The GS2 simulations also find the radially increasing Prandtl number profiles. However, while the simulated collisionality independence and radial dependences are in good agreement with the experimental ones, the simulated values of both $Rv_{\rm pinch}/\chi_\phi$ and P_r are lower than the experimental ones by a factor of 1.2–2. In particular, the Prandtl numbers from GS2 runs are lower by more than a factor of 1.5 than the experimental one throughout the radius, whereas the pinch numbers from GS2 runs actually reach values rather close to the experimental ones at $\rho > 0.6$. The reason for this quantitative difference in the magnitude of the P_r number and partly also in the pinch number between the GS2 runs and the experiments has not yet been identified. In earlier studies of a few JET H-mode pulses with NBI modulation, somewhat better agreement in the magnitude of the pinch and P_r numbers between the experiments and linear gyro-kinetic simulations with the GKW code [49] have been found [7].

3.2. Dependence of momentum pinch and Prandtl number on inverse density gradient length R/L_n

There is no simple way to perform a clean R/L_n scan in a tokamak without changing some other dimensionless parameter simultaneously. In particular, as already discussed in section 3.1, the strong coupling between the collisionality and R/L_n in H-mode plasmas makes the R/L_n scan without changing the collisionality virtually impossible to carry out. However, since no dependence of momentum transport coefficients on collisionality was found in the collisionality scan experiment as discussed in the previous section, it is possible to scan R/L_n by varying collisionality and assign the possible changes in momentum transport to be caused by R/L_n rather than collisionality.

The dependence of the Prandtl number on R/L_n is illustrated in figure 5. The single value of P_r attached to each shot is based on the average value of P_r between $0.4 < \rho < 0.8$. Also, R/L_n reflects the average value from the same radial range. The large range in R/L_n among the shots has been achieved mainly by varying collisionality, density and the amount of the NBI heating power. The magnetic field is 3.0 T and plasma current 1.5 MA for all the shots and the line-averaged density varied from 4.4×10^{19} m^{-2} to 8.4×10^{19} m^{-2}. It is evident in figure 5 that the Prandtl number does not depend on R/L_n as the scatter of the points is uniform. Typical error bars have been added for two of the shots. The variation in the error bar in the calculation of R/L_n is much smaller for the shots (such as the upper point with the error bar in figure 5) that have HRTS diagnostics measurements available than for the discharges with only Lidar Thomson scattering data (such as the lower point with the error bar in figure 5).

The red points in figure 5 are from linear GS2 simulations using the input data from 9 of the 12 experimental shots.

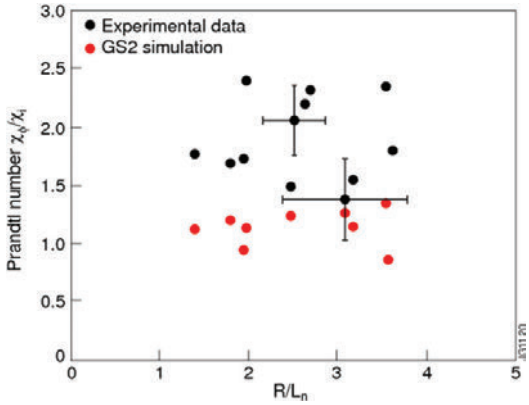

Figure 5. Experimental (black dots) and simulated (red dots) Prandtl numbers $P_r = \chi_\phi/\chi_i$, averaged over the range $0.4 < \rho < 0.8$, as a function of the inverse density gradient length R/L_n.

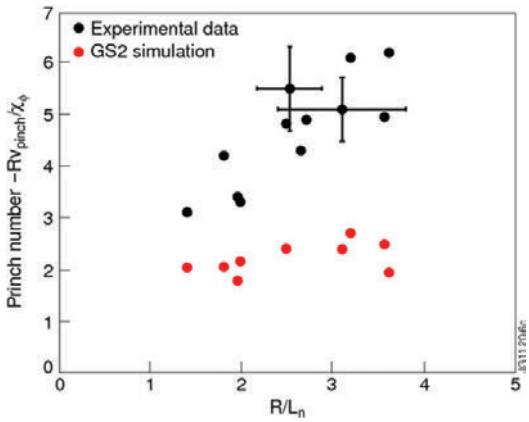

Figure 6. Experimental (black dots) and simulated (red dots) pinch numbers $-Rv_{\rm pinch}/\chi_\phi$, averaged over the range $0.4 < \rho < 0.8$, as a function of the inverse density gradient length R/L_n.

Consistent with experimental results, the Prandtl number is not found to depend on R/L_n by GS2. As already pointed out for the L-mode shots in section 3.1, the Prandtl numbers calculated by GS2 are lower than those of experiments. However, for the H-mode shots, the difference is typically smaller than a factor of 2 typically found for the L-mode shots.

While no dependence of the Prandtl number on R/L_n was found, a clear trend is found for the pinch number. This is illustrated in figure 6 where a strong dependence of the pinch number is plotted against R/L_n by the black points. Typical error bars originating from the analysis are shown for two cases, indicating that the dependence is clearly outside the error bars. For these shots, the NBI power and torque are significantly large (10–18 N m) and therefore, the intrinsic torque component is not believed to modify the conclusions. The present experimental evidence shows that intrinsic rotation is small on JET [13, 50, 51], around 10% or less of the NBI torque for the plasmas used in this density gradient length scan.

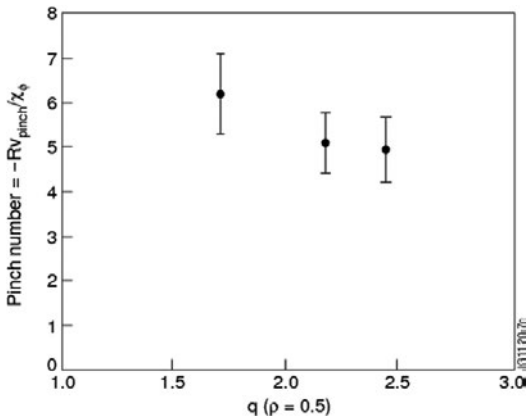

Figure 7. The experimental momentum pinch number $-Rv_{\rm pinch}/\chi_\phi$ with its error bars as a function of q value at mid-radius $\rho = 0.5$ from the 3-point q scan.

Similar to figure 5, the red points correspond to the GS2 simulations based on the experimental shots. GS2 runs also show an increase in $-Rv_{\rm pinch}/\chi_\phi$ with increasing $R/L_{\rm n}$ although the trend is much weaker than in the experimental data. The difference in the $R/L_{\rm n}$ dependence of the pinch number between the experiment and gyro-kinetic simulations is not fully understood. Preliminary simulations with GKW including the $E \times B$ shearing effect [52] have found that this mechanism produces a residual stress which is, however, too small to explain the difference between the predicted and measured pinch velocities. More extended investigations, also considering other residual stress mechanisms like the profile shearing effect [53, 54], are planned for future work.

Fitting a line through the experimental cloud of points, one obtains the following relation:

$$-Rv_{\rm pinch}/\chi_\phi \approx 1.2R/L_{\rm n} + 1.4. \quad (2)$$

The strong dependence of the momentum pinch on $R/L_{\rm n}$ has already been discussed earlier in theory [34]. What is also straightforward to conclude from the dependence above is that without knowing the inverse density gradient length, it will be challenging to estimate the momentum pinch number. When $R/L_{\rm n}$ ranges from 1 to 3 (typical values in present tokamak plasmas), $-Rv_{\rm pinch}/\chi_\phi$ ranges from 2.6 to 5, resulting in a large difference in rotation peaking. This strong dependence also has consequences to ITER predictions, discussed in more detail in section 5.

3.3. q-scan of the momentum pinch and Prandtl numbers

A 3-point q-scan was performed on JET. By keeping the magnetic field at $B = 3.0$ T, the variation in q was obtained firstly by increasing $I_{\rm p}$ from 1.5 MA to 2.5 MA and secondly by adding 3 MW of ICRF heating to delay current diffusion during and after the current ramp-up. The result of the scan is presented in figure 7 as a function of q at mid-radius. The variation of $R/L_{\rm n}$ within this 3-point q-scan in figure 7 was about 0.4, which should result in a change of 0.5 in the pinch number according to scaling (2). Therefore, the observed weak q dependence of the pinch number (larger than 1 unit in $-Rv_{\rm pinch}/\chi_\phi$ in figure 7) seems larger than the one induced by the difference in $R/L_{\rm n}$ between the high and low q shots. However, taking into account of the actual error bars as indicated in the plot, no solid conclusion can be drawn about the momentum pinch number dependence on q although the scan may suggest a possible weak dependence.

One should also note that while q is scanned here, the magnetic shear s is also varied, and the theory suggests in addition to the q dependence that $-Rv_{\rm pinch}/\chi_\phi$ depends also on s [34]. These two effects are challenging to separate from each other in the experiment. The Prandtl numbers for the same three shots are 1.55, 1.39 and 1.81, respectively, in the descending order of q as in figure 7. Therefore, one can conclude that no trend between the Prandtl number and q-profile was found within this scan.

4. Prandtl number in L-mode and H-mode plasmas

As already visible in figure 3, the Prandtl numbers are high in JET L-mode plasmas. They are typically above 2 outside mid-radius and can reach values up to 2.5. This is significantly larger than predicted by the early momentum transport fluid theory which gives Prandtl number to be 1 [55]. It is also somewhat larger than predicted by more recent gyro-kinetic simulations [56]. The gyro-kinetic simulations of the present JET L-mode discharges with GS2 also give Prandtl number profiles typically around unity, as shown in figure 4. There is clearly a quantitative disagreement between the experimental data and gyro-kinetic simulations although qualitatively, for example, the increasing P_r value as a function of the radius is well captured in simulations.

The relation of the Prandtl number between the L-mode and H-mode is studied more systematically here. The discharges chosen for the comparison have the same B, $I_{\rm p}$, $n_{\rm e}$ and NBI heating only. The two extreme cases with respect to P_r as far from each other as possible from this comparison are illustrated in figure 8 (left frame). For this extreme case, the Prandtl number in L-mode is more than 50% higher than in H-mode at all radii where the turbulent transport dominates over the neoclassical contribution. Looking into a larger set of JET NBI modulation shots, the trend that L-mode plasmas have higher Prandtl numbers than the H-mode ones is obvious, as shown in figure 8 (right frame). The Prandtl number of the highest L-mode shot and the one of the lowest H-mode shot are the ones plotted in the left frame. No similar trend for the pinch number is found between the L- and H-mode plasmas.

No obvious reason for the difference in P_r between L- and H-mode has been found so far. One candidate could be, as already discussed in section 3.1, that the L-mode shot could have more TEM driven transport and therefore, P_r, as compared with $\chi_{\rm i}$ would be higher. However, the linear GS2 simulations of these JET L-mode plasmas do find ITG as the dominant instability and by a large margin. This is not a surprise as these L-mode plasmas, heated with NBI only, have $R/L_{T_{\rm i}} \approx R/L_{T_{\rm e}}$ and $T_{\rm i} \approx T_{\rm e}$ and under these conditions, ITG always dominates. Another candidate could be the fact that if there are some non-NBI, intrinsic torque sources, their role could be larger in low NBI torque, low rotation L-mode plasmas. Residual stress has been proposed as a possible

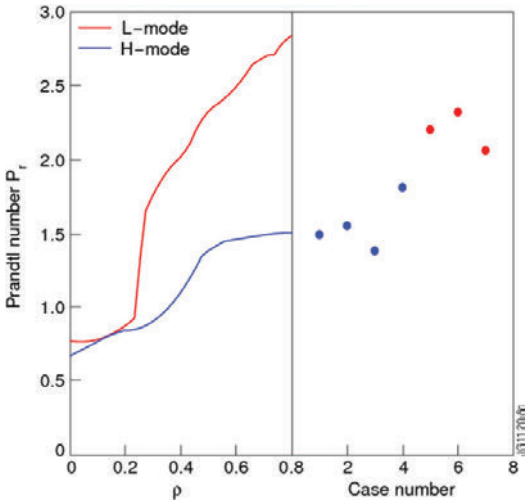

Figure 8. Comparison of the Prandtl number profiles in JET L-mode and H-mode plasmas (left frame) and a set of L-mode (red points) and H-mode (blue points) discharges (right frame) with the Prandtl number averaged over the radius $0.4 < \rho < 0.8$. Each point (case) in the right frame corresponds to a single analysed shot.

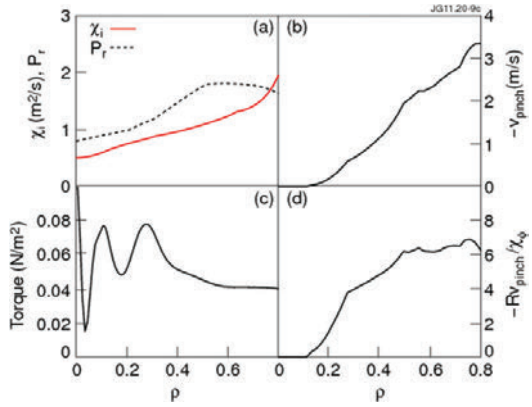

Figure 9. (*a*) The ion heat diffusivity and Prandtl number profile, (*b*) the pinch velocity, (*c*) the torque profile and (*d*) the pinch number profile used in the ITER simulations.

candidate to drive intrinsic rotation although its contribution in the core plasma may not be very large [57, 58]. However, if one assumes that its contribution would be the same in L-mode and H-mode plasmas, its relative importance and its possible effect on increasing spuriously the Prandtl number would be larger in low torque L-mode plasmas. This is because in this analysis method we have assumed NBI torque as the only torque source and its absolute value is typically of the order of 5 N m in L-mode plasmas while it is more like 15 N m in H-mode plasmas. Therefore, adding an extra intrinsic rotation or residual stress torque would modify the Prandtl and pinch numbers L-mode plasmas much more than in the H-mode ones.

5. Discussion of the consequences of these experimental results in view of rotation in ITER

Predicting the toroidal rotation profile in ITER is a challenging task. In recent years, predictive transport simulations of toroidal rotation using first-principles transport models have been performed to tackle this task [59, 60]. However, although serving as a good base for the starting point of the ITER rotation predictions, a number of simplified assumptions for momentum transport and torque sources have often been adopted in these modelling efforts. In particular, the assumptions that $\chi_\phi = \chi_i$, that there is no momentum pinch and that the NBI is the only torque source, may easily lead to qualitatively incorrect rotation predictions.

In this work, we take a different approach and use the Prandtl and pinch number profiles based on the scans of the parametric dependences on JET described in the previous sections. The main emphasis is to clarify the role of strong inward pinch under a variety of torque profiles and a variety of edge rotation values in shaping the toroidal rotation profile in ITER. However, it is to be noted already at this point that these simulations will not be the final ITER predictions for the toroidal rotation profile, but rather to demonstrate the key role of both the inward momentum pinch and the boundary conditions of the rotation in any realistic ITER rotation simulations. Important factors to make the final realistic ITER rotation prediction that we are still neglecting in this study are for example any non-NBI, intrinsic torque sources [10, 11], residual stress type of momentum flux terms [26, 58], braking effects for example due to 3D effects from RMP coils to suppress ELMs [17] and any consideration on what the edge rotation will be in ITER. To demonstrate the crucial role of the edge rotation boundary condition, an edge rotation scan is performed. Another example of a sink term neglected here is the TBM that may have a large influence on both the edge and core rotation in ITER, at least it is suggested by the DIII-D TBM experiments [19].

The rotation modelling philosophy in this study is that the temperature and density profiles are taken from the ITER reference scenario 2 (15 MA baseline scenario) specifications [61]. Only the equation for the toroidal rotation is solved in the JETTO transport code [40, 62] while the rest is taken from ITER reference scenario 2. GLF23 transport model [63] is used to calculate the ion heat diffusion coefficient χ_i from the given temperature and density profiles, shown in figure 9(*a*). The NBI torque profile, assuming the standard ITER specifications (ITER scenario 2 at density of 10^{20} m^{-3}), i.e. 33 MW of input power using 1 MeV negative ion beam source with a realistic ITER magnetic ripple background, has been calculated with the ASCOT code. The real NBI geometry with two injectors, one more on-axis and one more off-axis, have been used. This torque profile with two separate peaks originating from the two injectors is presented in figure 9(*c*).

For momentum transport, we take the Prandtl number and momentum pinch profiles from the high current (I_p = 2.5 MA, B = 3 T), low q, low collisionality (ν^* = 0.04) JET discharge no 73702. This can be considered to be the closest discharge, among those shots where the NBI modulation technique has been exploited, to ITER with respect to dimensionless parameters, but is by no means representing a perfect match with ITER numbers. Note that one of the

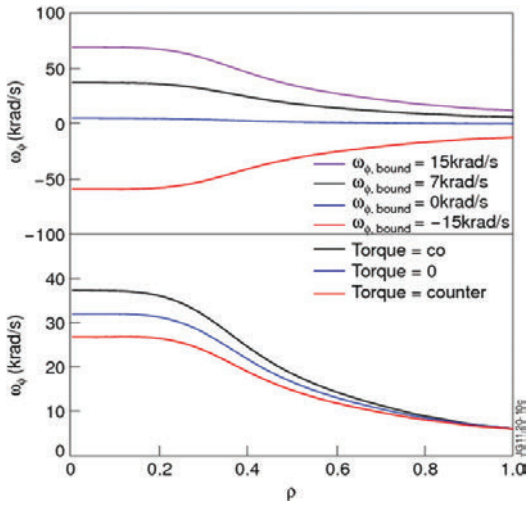

Figure 10. (*a*) The predictive toroidal rotation simulations for the ITER baseline scenario using various boundary conditions for the edge rotation. (*b*) As in (*a*) at $\omega_{\phi,\text{bound}} = 7\,\text{krad}\,\text{s}^{-1}$, but for co-, counter- and balanced (zero) NBI torque options.

dimensionless parameters most different in ITER than on JET is collisionality, however, based on the results presented in section 3.1, there is a good reason to believe that the momentum pinch and Prandtl numbers are independent of collisionality also in ITER. The Prandtl number profile used in the predictive simulations is shown in figure 9(*a*) and the pinch number profile in figure 9(*d*). This pinch number profile corresponds to the JET plasma with the inverse density gradient lengths of around $R/L_\text{n} \approx 3$–3.5 as illustrated in figure 6. For a comparison, the ITER standard scenario can be expected to have density peaking at mid-radius of $R/L_\text{n} = 2$–2.5 [43] as predicted consistently by both empirical scalings [64–66] as well as by theory-based transport simulations [67]. The actual pinch velocity in this ITER plasma can be calculated from the pinch number profile in figure 9(*d*), and is presented in figure 9(*b*).

Based on the modelling assumptions presented above, two scans of predictive simulations of toroidal rotation were performed. In the first scan, the boundary condition for the toroidal rotation was varied between $\omega_{\phi,\text{bound}} = -15\,\text{krad}\,\text{s}^{-1}$ and $15\,\text{krad}\,\text{s}^{-1}$. This boundary rotation of $15\,\text{krad}\,\text{s}^{-1}$ in ITER corresponds to normalized Mach Alfvén velocity $M_\text{A} = 0.0077$ on top of the H-mode pedestal $\rho = 0.95$ when using the profiles from the ITER reference scenario 2. This range of uncertainties in the edge rotation ($\omega_{\phi,\text{bound}} = -15$–$15\,\text{krad}\,\text{s}^{-1}$) can be easily caused for example by ripple [9], TBMs [19], ELMs [20], neutrals [21], interaction with SOL flows, for example seen between the upper and lower null configurations [22, 23] or other unknown edge torque sources.

The predicted toroidal rotation profile for each of the four boundary conditions is presented in figure 10(*a*). There are several interesting points worth commenting on. Firstly, the rotation with the zero-slip boundary condition (blue curve) is very close to zero throughout the whole radius. This suggests that the NBI torque deposited in the core region alone, at least with the present assumption for the Prandtl and pinch number profiles, is not able to create a significant toroidal rotation in ITER. On the other hand, when the boundary condition is increased to $\omega_{\phi,\text{bound}} = 7\,\text{krad}\,\text{s}^{-1}$ (black curve) or $\omega_{\phi,\text{bound}} = 15\,\text{krad}\,\text{s}^{-1}$ (magenta curve), significant toroidal rotation is predicted in the plasma core region, corresponding to $M_\text{A} = 0.03$ in the plasma centre with $\omega_{\phi,\text{bound}} = 15\,\text{krad}\,\text{s}^{-1}$. Concerning the NBI torque in ITER, it is, however, well possible that the NBI torque will affect the rotation value at the edge, either by a direct edge torque source or by the momentum flux created in the core. Studying the influence of the NBI torque, or any other edge torque source, on edge rotation is beyond the scope of this paper and thus left for future work. Therefore, no solid conclusion can yet be drawn on the overall role of the NBI torque in ITER. Another interesting point in figure 10 is that when the boundary condition is set to counter-rotation at the same magnitude of $\omega_{\phi,\text{bound}} = -15\,\text{krad}\,\text{s}^{-1}$ (red curve), the rotation becomes almost as much counter as it was co with $\omega_{\phi,\text{bound}} = 15\,\text{krad}\,\text{s}^{-1}$ boundary condition. This shows again that the core NBI torque has a minor role in directly determining the core toroidal rotation profile provided that the pinch number is large enough—note here the possibly important role of the NBI torque in determining the magnitude of the edge rotation which is not taken into account. The minor effect of the core NBI torque is illustrated further in figure 10(*b*), as the rotation profile does not change very much whether the NBI torque is co, balanced or counter (to note that counter-I_p or balanced NBI is not an option considered currently for ITER). Also note here that in these simulations, the boundary value of the rotation has been kept fixed independent of the direction of the NBI torque, and surely the direction of the NBI torque would have some impact on edge rotation. To sum up these ITER simulations, it is evident that the knowledge of the boundary condition, of course in addition to the knowledge of the magnitude of the pinch, is vital when the rotation profile is predicted to ITER plasmas. This is most obvious when the inward pinch is large. If the pinch number is small in ITER, for example as low as 2 or below around the mid-radius, then the core torque sources, such as NBI or RF driven or intrinsic ones, still play a major role in determining the shape of the core rotation profile.

6. Summary and conclusions

The NBI modulation technique has been exploited on JET to study parametric dependences of both the momentum pinch and the Prandtl number. This method is a powerful experimental tool to separate the diffusive and convective components of the momentum flux. The plasmas studied in all of the scans are dominated by ITG modes, therefore making the concept of Prandtl number, unambiguous. The torque calculations have been performed either with TRANSP or ASCOT and the results have been benchmarked against each other. In the experimental planning and transport analysis, great care has been taken in getting rid of MHD modes, such as sawtooth and ELMs, and equilibrium remapping due to plasma oscillations caused by the NBI modulation.

A dedicated collisionality scan was performed by keeping the other dimensionless quantities (β_N, ρ^*, q, T_e/T_i) constant. No change in the pinch number was observed when the

collisionality was varied by a factor of 4 within the scan. In addition, no dependence of the Prandtl number on collisionality was found. The pinch number was found to decrease weakly with increasing q, but this dependence is just within the error bars so that no solid conclusions can be drawn. The Prandtl number did not depend on q.

Within the R/L_n scan, a strong dependence for the pinch number on the inverse density gradient length was observed, $-Rv_{pinch}/\chi_\phi \approx 1.2R/L_n + 1.4$. This dependence is consistent with the JET rotation database study where a similar dependence of the pinch number on R/L_n is reported in [68]. Also, a statistical approach applied to the JET rotation database yields a similar trend [69]. Within the same R/L_n scan, the Prandtl number was not found to be sensitive to R/L_n in these JET experiments.

GS2 simulations are in good qualitative agreement with JET experimental results, i.e. the pinch and Prandtl numbers are found to be independent of collisionality and an increase in the pinch number with increasing R/L_n is reproduced. In some cases, such as the magnitude of the pinch number in the collisionality scan, a quantitative agreement is obtained. However, in many cases, such as the magnitude of the pinch number in the R/L_n scan or the Prandtl number in both the collisionality and R/L_n scans were significantly smaller in GS2 simulations than in the experiments. Concerning the pinch number in the R/L_n scan, one can note that the same simulations with the GKW code result consistently in about 10% higher pinch numbers than those calculated with GS2, making thus the discrepancy between the experiment than simulations somewhat smaller. Qualitatively, however, the trend of the pinch number with R/L_n remains similar between the two codes, i.e. still quantitatively smaller than found in the experiments.

In order to try to pin down possible reasons for the discrepancy between the experimentally found strong trend of the pinch number on R/L_n and the weaker one found in the GS2 simulations, one can first look for possible additional torque source terms or terms in the momentum flux. Based on the experimental intrinsic rotation data in JET, it is relatively easy to conclude that the intrinsic rotation is always quite small, less than $\pm 30\,\mathrm{km\,s^{-1}}$, and in fact, usually it is much smaller than that [13, 14]. This is to be compared with the NBI modulation H-mode discharges in these scans that have typically central rotation values of about 150–200 $\mathrm{km\,s^{-1}}$. As a consequence, the intrinsic rotation drive term seems to be an order of magnitude smaller at least in JET H-mode shots. However, it cannot be completely excluded experimentally that the residual stress term, for example due to a stronger H-mode pedestal in the higher power NBI modulation shots, could affect more the rotation than in the lower power intrinsic rotation studies (ICRH heated plasmas on JET cannot have the typical 12–14 MW of heating power that we have in NBI modulated shots). In order to test this effect, however, we have added an extra arbitrary torque term in addition to the pinch and Prandtl number in the transport analysis with JETTO for several JET shots. The result clearly shows that the fit between the experimental and JETTO simulated amplitude, phase and steady-state rotation is not or only marginally improving by adding such a term describing the residual stress. While the experimental evidence suggests that the effect of the residual stress term in the plasma core is relatively small, it may still have an important contribution to the rotation profile outside $r/a > 0.8$ which has not been analysed at all in this study where the boundary conditions are matched at $r/a = 0.8$.

In L-mode plasmas, there is certainly more room for the residual stress or other non-NBI torque terms to modify the deduced pinch and Prandtl numbers as the typical value of rotation is around $100\,\mathrm{km\,s^{-1}}$ with 5–6 MW of NBI power including the modulation. Therefore, if the residual stress drive stays the same as in H-mode, its impact can be significantly larger in L-mode plasmas. On the other hand, experimental evidence from DIII-D shows that it is just at the pedestal where the intrinsic torque drive is strongest [58]. In any case, adding co-torque in the pedestal and counter torque in the core, as found on DIII-D, would indeed decrease the deduced Prandtl number in the core (in the region of $0.3 < \rho < 0.8$) in the L-mode plasmas and thereby making it more similar to the ones in H-mode (see figure 8). However again, in the experimental JETTO transport analysis adding an extra torque term does not significantly improve the simulated amplitude, phase and steady-state with respect to the experimental ones, indicating that the residual stress may not be the key to resolve the discrepancy in the Prandtl number between the L- and H-mode. It is possible that the disagreement between the high experimental Prandtl numbers and the simulated GS2/GKW ones become closer to each other when taking into account the neoclassical $E \times B$ shear effect on the GS2/GKW Prandtl number calculation. Preliminary GKW simulations with the neoclassical $E \times B$ shear effect suggest at least an increase of Prandtl number for a few cases, but a more detailed analysis of the role of the residual stress term as a whole in JET H- and L-mode plasmas is left for future work.

Another possibility making the Prandtl number to be different in JET L- and H-mode plasmas is that L-mode plasmas are always in a different parameter regime as already discussed in section 3.1. In particular, the electron temperature and R/L_{T_e} tend to be higher with respect to the ion temperature and R/L_{T_i} in L-mode plasmas. This fact points towards a possible larger drive from TEM with respect to ITG and consequently, the concept of the Prandtl number being a ratio of momentum diffusivity to ion heat diffusivity could be less unambiguous. However, although a larger TEM drive is indeed found in GS2 simulations in JET L-mode versus H-mode pulses, the difference is so small that at least based on these simulations, this does not look like a possible explanation to resolve the Prandtl number discrepancy.

Based on the results from these parametric scans of the pinch and Prandtl numbers, one can conclude that the inward pinch will have a significant impact on rotation profile in ITER provided that some rotation sources are available at the edge of the plasma. The edge rotation has to be finite such that the inward pinch can be effective to make the plasma rotation peaked. With a finite edge rotation and a large enough inward pinch, core rotation sources may not in the end play such an important role in ITER than in present tokamaks. However, in predicting the rotation profile and magnitude for ITER, large uncertainties certainly remain, not just due to uncertainties in edge rotation and scaling of the pinch, but also due to uncertainties in core and edge sink terms. In particular, braking effects from resonant magnetic perturbation or other 3D effects

like TBMs may give large uncertainties in any extrapolation of the rotation profile for future tokamaks. Moreover, some MHD modes, such as Alfvén eigenmodes or NTMs, not discussed in this paper, can influence the rotation profile in ITER and furthermore, also fusion born fast alpha particles may have an effect on rotation to be taken into account [70]. In conclusion, while it seems plausible that the rotation profile will be peaked in ITER, the absolute magnitude of the toroidal rotation still remains challenging to predict with the present uncertainties in the edge rotation, in sources/sinks and in the exact extrapolation of the inward momentum pinch.

Acknowledgments

This work was supported by EURATOM and carried out within the framework of the European Fusion Development Agreement. The views and opinions expressed herein do not necessarily reflect those of the European Commission.

References

[1] Biglari H., Diamond P.H. and Terry P. 1990 *Phys. Fluids* B **2** 1
[2] Miller R.L. *et al* 1994 *Phys. Plasmas* **1** 2835
[3] Burrell K.H. 1997 *Phys. Plasmas* **4** 1499
[4] Mantica P. *et al* 2009 *Phys. Rev. Lett.* **102** 175002
[5] Garofalo A.M. *et al* 2001 *Nucl. Fusion* **41** 1171
[6] Buttery R.J. *et al* 2011 Cross-machine scaling of neoclassical tearing modes thresholds with rotation *Nucl. Fusion* submitted
[7] Mantica P. *et al* 2010 *Phys. Plasmas* **17** 092505
[8] Salmi A.T. *et al* 2011 *Plasma Phys. Control. Fusion* **53** 085005
[9] de Vries P.C. *et al* 2008 *Nucl. Fusion* **48** 035007
[10] Rice J.E. *et al* 2007 *Nucl. Fusion* **47** 1618
[11] deGrassie J.S. 2009 *Plasma Phys. Control. Fusion* **51** 124047
[12] McDermott R.M. *et al* 2011 *Plasma Phys. Control. Fusion* **53** 035007
[13] Eriksson L.-G. *et al* 2009 *Plasma Phys. Control. Fusion* **51** 044008
[14] Nave M.F.F. *et al* 2010 *Phys. Rev. Lett.* **105** 105005
[15] Lin Y. *et al* 2011 ICRF mode conversion flow drive in D(3He) plasmas on JET *Plasma Phys. Control. Fusion* submitted
[16] Lin Y. *et al* 2008 *Phys. Rev. Lett.* **101** 235002
[17] Sun Y. *et al* 2010 *Plasma Phys. Control. Fusion* **52** 105007
[18] Garofalo A.M. *et al* 2008 *Phys. Rev. Lett.* **101** 195005
[19] Schaffer M.J. *et al* 2011 *Nucl. Fusion* **51** 103028
[20] Versloot T. *et al* 2010 *Plasma Phys. Control. Fusion* **52** 045014
[21] Versloot T. *et al* 2011 *Plasma Phys. Control. Fusion* **53** 065017
[22] Rice J. *et al* 2005 *Nucl. Fusion* **45** 251
[23] LaBombard B. *et al* 2004 *Nucl. Fusion* **44** 1047
[24] Diamond P.H. *et al* 2008 *Phys. Plasmas* **15** 012303
[25] Dominguez R.R. *et al* 1993 *Phys. Fluids* B **5** 3876
[26] Peeters A.G. *et al* 2011 *Nucl. Fusion* **51** 094027
[27] Yoshida M. *et al* 2007 *Nucl. Fusion* **47** 856
[28] Tala T. *et al* 2007 *Plasma Phys. Control. Fusion* **49** B291
[29] Tala T. *et al* 2009 *Phys. Rev. Lett.* **102** 075001
[30] Tardini G. *et al* 2009 *Nucl. Fusion* **49** 085010
[31] Solomon W.M. *et al* 2009 *Nucl. Fusion* **49** 085005
[32] Solomon W.M. *et al* 2008 *Phys. Rev. Lett.* **101** 065004
[33] Kaye S.M. *et al* 2009 *Nucl. Fusion* **49** 045010
[34] Peeters A.G. *et al* 2007 *Phys. Rev. Lett.* **98** 265003
[35] Hahm T.S. *et al* 2007 *Phys. Plasmas* **14** 072302
[36] Peeters A.G. *et al* 2009 *Phys. Plasmas* **16** 062311
[37] Negus C.R. *et al* 2006 *Rev. Sci. Instrum.* **77** 10F102
[38] Goldston R.J. *et al* 1981 *Comput. Phys.* **43** 61
[39] Heikkinen J.A. *et al* 2001 *J. Comput. Phys.* **173** 527
[40] Genacchi G. *et al* 1988 JETTO: a free boundary plasma transport code (basic version) *Rapporto ENEA RT/TIB* 1988(5)
[41] Luce T.C. *et al* 2008 *Plasma Phys. and Control. Fusion* **50** 043001
[42] Weisen H. *et al* 2005 *Nucl. Fusion* **45** L1
[43] Angioni C. *et al* 2009 *Plasma Phys. Control. Fusion* **51** 124017
[44] Kotschenreuther M. *et al* 1995 *Comput. Phys. Commun.* **88** 128
[45] Giroud C. *et al* 2008 *Rev. Sci. Instrum.* **79** 525
[46] Dorland W. *et al* 2000 *Phys. Rev. Lett.* **85** 5579
[47] Kluy N. *et al* 2009 *Phys. Plasmas* **16** 122302
[48] Bourdelle C. *et al* 2007 *Phys. Plasmas* **14** 112501
[49] Peeters A.G. *et al* 2009 *Comput. Phys. Comm.* **180** 2650
[50] Nave M.F.F. *et al* 2010 *Phys. Rev. Lett.* **105** 015005
[51] Nave M.F.F. *et al* 2011 JET intrinsic rotation studies and predictions for ITER *Plasma Phys. Control. Fusion* submitted
[52] Casson F.J. *et al* 2009 *Phys. Plasmas* **16** 092303
[53] Waltz R.E. *et al* 2011 *Phys. Plasmas* **18** 042504
[54] Camenen Y. *et al* 2011 *Nucl. Fusion* **51** 073039
[55] Mattor N. *et al* 1988 *Phys. Fluids* **31** 1180
[56] Peeters A.G. *et al* 2005 *Phys. Plasmas* **12** 072515
[57] Diamond P.H. *et al* 2009 *Nucl. Fusion* **49** 045002
[58] Solomon W. *et al* 2011 *Nucl. Fusion* **51** 073010
[59] Budny R.V. *et al* 2008 *Nucl. Fusion* **48** 075005
[60] Halpern F.D. *et al* 2008 *Phys. Plasmas* **15** 062505
[61] Ikeda K. *et al* 2007 *Nucl. Fusion* **47** S18
[62] Tala T.J.J. *et al* 2000 *Nucl. Fusion* **40** 1635
[63] Waltz R.E., *et al* 1997 *Phys. Plasmas* **4** 2482
[64] Weisen H. *et al* 2006 *Plasma Phys. Control. Fusion* **48** A457
[65] Angioni C. *et al* 2007 *Nucl. Fusion* **47** 1326
[66] Greenwald M. *et al* 2007 *Nucl. Fusion* **47** L26
[67] Pereverzev G.V. *et al* 2005 *Nucl. Fusion* **45** 221
[68] de Vries P.C. *et al* 2010 *Plasma Phys. Control. Fusion* **52** 065004
[69] Weisen H. *et al* Probable identification of the Coriolis momentum pinch in JET *38th EPS Conf. (Strasbourg, France, 27 June–1 July 2011)* paper O4.120
[70] Honda M. *et al* 2011 *Nucl. Fusion* **51** 073018